The Whole Sky Imager - A Year of Progress

J. E. Shields, and M. E. Karr
Marine Physical Laboratory
Scripps Institution of Oceanography
University of California, San Diego
San Diego, California

T. P. Tooman
Sandia National Laboratories
Livermore, California

D. H. Sowle, and S. T. Moore
Mission Research Corporation
Santa Barbara, California

Abstract

Much progress has been made this last year in realizing the potential of the Whole sky imager (WSI). Two imagers are deployed (at the Southern Great Plains [SGP] site and the Surface Heat Budget of the Arctic Ocean [SHEBA]), two are being prepared for deployment in the Tropical Western Pacific (TWP), and more are in production. Data products now include daytime thick cloud fraction and calibrated radiance. Night cloud fraction and daytime thin cloud fraction retrievals are in development.

Introduction

The day/night WSI is a 16-bit digital imaging system that acquires images of the full sky (2π hemisphere) under both day and night conditions, in order to assess cloud fraction, cloud morphology, and radiance distribution. The WSI measures the sky radiance in approximately 185,000 directions simultaneously using a 512 x 512 charge-coupled device (CCD) sensor. This results in a 34 micro steradian field of view (FOV) in each direction, to cover the full 2π steradian dome. The WSI has a large dynamic range, such that high resolution data may be acquired under daylight, moonlight, and starlight. Images are acquired in the visible and near infrared (NIR), with filters at 450 nm (blue), 650 nm (red), and 800 nm (NIR) under sunlight or moonlight. An open hole visible filter is used under starlight. The image acquisition interval is user selected, with intervals such as 1 minute or 10 minutes between image sets. To date, the Atmospheric Radiation Measurement (ARM) Program has opted to use either 10-minute intervals or 2-minute intervals, due to the large quantities of data generated by the instrument.

A picture of the instrument fielded at the Oklahoma Cloud and Radiation Testbed (CART) site is shown in Figure 1. The primary features seen in this figure are the environmental housing that protects the sensor and electronics, the optical dome, and the solar occultor that shades the optics. Figure 2 shows a daytime image and the corresponding cloud decision image generated by the system. In both images, the center of the image is the zenith, and the edges are the horizon. In the cloud decision image, opaque cloud is indicated by white or gray, no cloud (clear or haze) is blue, and the yellow is a preliminary thin cloud determination. A sample starlight image is shown in Figure 3. Note that even partially transparent clouds are being successfully detected at night; i.e., the stars may be

Figure 1. Day/night whole sky imager fielded at SGP CART site. (For a color version of this figure, please see *http://www.arm.gov/docs/documents/technical/conf_9803/shields-98.pdf.*)
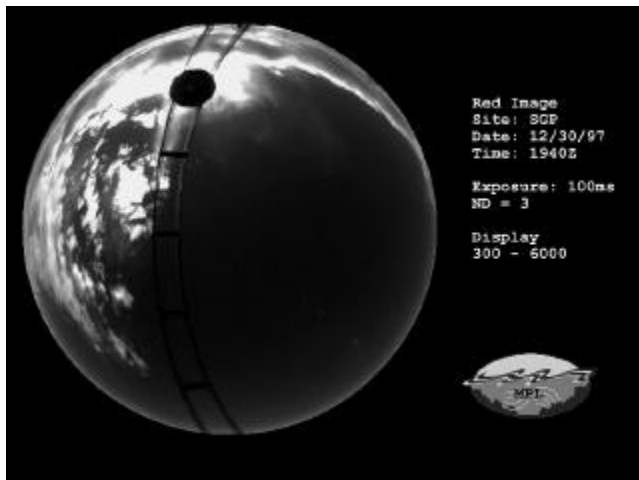
Figure 2a. Raw red image. A subset of the radiance range is shown. The edge is the horizon and the center is the zenith.
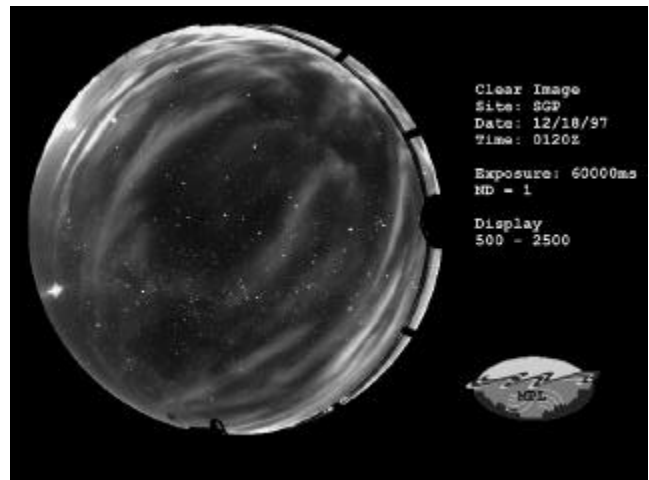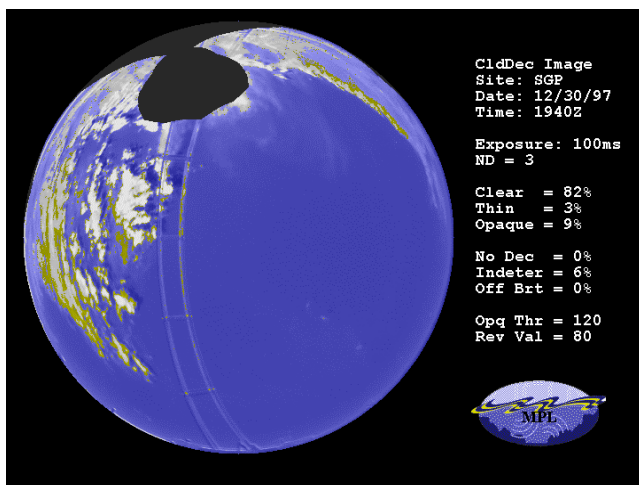

Figure 2b. Cloud decision image. This shows a gray rendition of the normal colored image output by the cloud decision algorithm which decides whether clouds are present within each pixel. The blocked area is an indeterminate region. (For a color version of this figure, please see *http://www.arm.gov/docs/ documents/technical/conf_9803/shields-98.pdf.*)

detected through some of the clouds. It should be noted that this rendition only shows a small part of the detail visible in the original full size image.

Instrument Description

The day/night WSI was developed over many years by the University of California, San Diego's (UCSD's) Marine Physical Laboratory (MPL). The earliest generation of

Figure 3. Starlight image acquired with no moon and thin clouds. The Milky Way is across the image just below the center.

WSIs developed by this group consisted of automated remote-controlled cameras viewing a silvered dome. These were developed under Air Force funding and used in the 1950s and 1960s. In the late 1960s, we converted from a silvered dome to a fisheye lens with superior imaging, stability, and stray light characteristics. This was supplemented by a scanning radiometer for acquiring absolute radiance. In the early 1980s, we developed the first digital WSI, using a solid state CID camera and fisheye lens. These systems were fielded at several locations acquiring data once a minute for 2 years, under Air Force sponsorship (Johnson et al. 1989, 1991). The first day/night WSIs were developed in the early 1990s under joint sponsorship from the Air Force, Navy, and Army (Shields et al. 1993). They have been adapted to the ARM Program at the MPL under U.S. Department of Energy (DOE) sponsorship and Sandia National Laboratory (SNL) mentorship (Shields et al. 1998).

The day/night WSI is ground based, and acquires the naturally occurring radiances of the sky and clouds. The primary optical element is a fisheye lens with a 181° field of view (which images from the zenith to just below the horizon at zenith angle 90.5°). The light is filtered by spectral and neutral density filters, and transferred via a tapered fiber optic bundle (with approximately 10^6 optical fibers) to the CCD. The tapered fiber optic bundle provides superior throughput and image quality in comparison with the lens relay approach used in the earlier day WSI.

The CCD camera, provided by Photometrics, is a very low noise 16-bit camera. Typical instrument noise (readout and dark current) is approximately 0.1% of the signal in the daytime. At night, under the darkest conditions with no

moon at a 1-minute exposure, instrumental noise is approximately 1% of the signal of the background sky between stars, and a much lower fraction of the star radiance signal. The camera, in combination with the filter and exposure selection by the system, yields a dynamic range about 10^{10}. That is, radiances can be measured from approximately 3×10^{-7} to 7×10^{2} (red) or 6×10^{3} (blue) Watt/Ωm$^{2}\mu$m.

The system is controlled by a PC base controller, with electronics developed at MPL for manual or automated control. Data are archived on magneto optical disks and also transferred via network to the sponsor's site computer (the site data system in Oklahoma and the ADaM at other networked sites). Algorithms programmed into the instrument provide flux control to keep data onscale even during quickly changing times such as sunset. Cloud algorithms yielding images, as shown in Figure 2, identify the presence of opaque clouds on a pixel-by-pixel basis; these are resident on the WSI and also have been transferred to the site computer in Oklahoma for near real-time processing of the data.

The environmental housing seen in Figure 1 is designed to keep the camera and electronics cool. Self-diagnostic indicators are also included in this housing. The arc seen in Figure 1 provides shading for the optical system. Even though the camera would not be damaged by direct sunlight, this shading is desirable because it minimizes stray light especially near the sun; one of the advantages of a fisheye lens system is the ability to shade even the primary optics.

Recent WSI Upgrades and Progress

In the last year, primary goals mentored by SNL have included providing an instrument for the Arctic environment, networking the instruments so that they could be fielded at the remote sites, completing the conversion (from PC to Sun) of the opaque cloud decision algorithms so the data can be processed at the Pacific Northwest National Laboratory (PNNL) or the sites, and providing radiance distributions. In addition, work on the upgrade of the thin cloud algorithm, analysis of the radiance distribution, and development of daylight thin cloud decision algorithms and starlight cloud decision algorithms is in progress.

Hardware Enhancements

During the year or so prior to the ARM meeting, a primary development was the adaptation of the WSI for the Arctic environment, and the fielding of the WSI at SHEBA.

Adaptations included hardware modifications such as stronger and more accessible leveling legs to enable convenient leveling on the ice breaker, and enhanced heating capability in the environmental housing. Software modifications included converting the system to read the changing latitude and longitude and ship orientation from the global positioning system (GPS), in order to properly compute the sun or moon position for occultor positioning and flux control. Following deployment, there was an initial problem with water vapor over approximately 30% of the dome. This was corrected by using a different type of gasketing on the optical dome. The system has otherwise performed quite well.

Several upgrades to the WSI hardware have been accomplished during the last year. Most importantly, the hardware was upgraded to enable networking of the instruments with the site computers. The networking hardware was fielded on two instruments at the Sandia test site in Albuquerque in September 1997, and at the Oklahoma site in October 1997, and has worked very well. The North Slope of Alaska (NSA) instrument will be networked after the SHEBA deployment.

Other changes to the systems this fall included changing to magneto optical disks for the backup archival (which supplements the archival via network), since the 8-mm tape drives had not proved as reliable as anticipated. At the same time, a fourth spectral filter, in the NIR at 800 nm, was added to the systems. At 800 nm, the Mie scattering of the aerosol (haze) is expected to be somewhat lower than at 650 nm under many conditions, and the smallest aerosol droplets behave more as Rayleigh scatterers. This would enhance the radiance contrast between the thin clouds and the sky, resulting in the detection of clouds of lesser optical density. In addition, this extra wavelength provides an additional degree of freedom in cloud detection algorithm development.

Data Processing Enhancements

One of the major points of progress this year was completion of the conversion of the original PC version of the cloud algorithm provided by MPL to run on the Sun computers at PNNL. This conversion was accomplished by PNNL personnel. At this time, most of the existing SGP data has been processed through this opaque cloud algorithm, and is available to the science team. In addition, the raw images have been processed through the Window algorithm (an algorithm for displaying the 16-bit images), in order to provide images that may be visually interpreted by the science team members. The data products currently available to the science team are summarized below.

- 16-bit raw data (red, blue, N/R, clear)
- "windowed" 8-bit red and clear images
- Cloud fraction files - opaque
- Cloud decision images - opaque

One of the primary capabilities of the instrument is the determination of the distribution of absolute radiance in Watt/$\Omega m^2 \mu m$ as a function of position in the sky, spectral filter, and time. The instruments are calibrated in-house prior to fielding, and during this year programs were developed to apply these calibrations to the field data. These will be discussed in more detail in the section on "Calibrated Radiances." Currently, the beta version of this software is available. Evaluation of the radiances in comparison with models has begun, and is also discussed in "Calibrated Radiances."

Several new data products are envisioned for the future, as shown below.

- Calibrated radiance images
- Quick look movie
- Zenith radiance
- Thin cloud fraction
- Cloud fraction at night

Primary among them is the thin cloud fraction. The current cloud fraction is computed using the opaque cloud algorithm, as discussed in the section on "Cloud Decision Algorithms." Current opaque cloud decision algorithms are based on the relative red/blue ratio. More sophisticated thin cloud decision algorithms are based on these ratios and a library of site-dependent, angularly dependent clear-sky ratios. These thin cloud decision algorithms are used in the cloud decision images (as in Figure 2) which are available to the science team. Currently, work is under way to upgrade the thin cloud algorithms, and then provide the thin cloud fraction in addition to the opaque cloud fraction. In addition, work is under way on the development of starlight cloud decision algorithms.

Calibrated Radiances

As noted above, one of the capabilities of the WSI is the determination of the absolute radiance distribution. The fisheye lens directs the light from different directions onto different pixels in the image plane, and the signal of each pixel may be calibrated to yield a determination of the absolute radiance, in Watt/$\Omega m^2 \mu m$, in that direction. The FOV for each pixel is approximately 34 micro-steradians. Thus, this radiance product is equivalent conceptually to a radiance distribution determined by a scanning radiometer, except that all radiances are acquired simultaneously (at 185,000 points) and at very high spatial resolution.

Calibration of the WSI

The overall sensitivity is determined by the lens, the transmittance of the various filters, the throughput of the optical fiber bundle, and the quantum efficiency of the CCD chip. The primary calibrations measured on the system are as follows.

Spectral Sensitivity of Chip and Transmittance of Filters: These spectral curves are used in conjunction with the calibration lamp spectral irradiance to compute the effective lamp irradiance in the filters used by the WSI. These effective irradiances are in turn an input to the processing of the absolute calibrations.

Dark Calibration: This characterizes the pixel-to-pixel variations in the zero signal (no light) offset.

Flat Field Calibration: This characterizes the pixel-to-pixel variations in the system gain.

Pixel Variance Calibration: This characterizes the sensor noise performance, for optimization of exposure selection in the flux control algorithm.

Linearity: This characterizes the relative system response to changing exposure and changing light levels.

Absolute Radiance Calibration: This determines the absolute radiance response as a function of filter selection.

Off-Axis Rolloff: This determines the off-axis effects of optical Fresnel losses and solid angle per pixel changes.

Geometric Angular Calibration: This characterizes zenith angle and azimuth angle in object space as a function of pixel in image space. It can be further enhanced through the use of star fields as the calibration source once the instrument is fielded.

To apply the calibration data to field data, a pixel-dependent dark image and flat image correction are made. The linearity is not currently applied because the system is linear to better than 0.5% over most of its range, but it may be applied in future upgrades to the software. The absolute radiance calibration consists of a single factor that is applied to each pixel within the entire image and depends on the filter selection and exposure. The rolloff is a zenith-angle dependent correction. The geometric calibration is used in various software to provide the position of each pixel in object space.

Sample Calibrated Data

An example of the changes in the absolute radiance near the zenith over a 24-hour period are shown in Figure 4. These data were acquired under generally clear skies, with occasional scattered cirrus clouds. The y axis is the log of the radiance in Watt/$\Omega m^2\mu m$, and the x axis is the Greenwich time in hours. The plot starts right after sunset, as the red and blue radiances are dropping quickly. There is a period of starlight, and then the radiance starts to rise as the moon nears the horizon and rises. The radiances change quickly during the sunrise, peaking near noon.
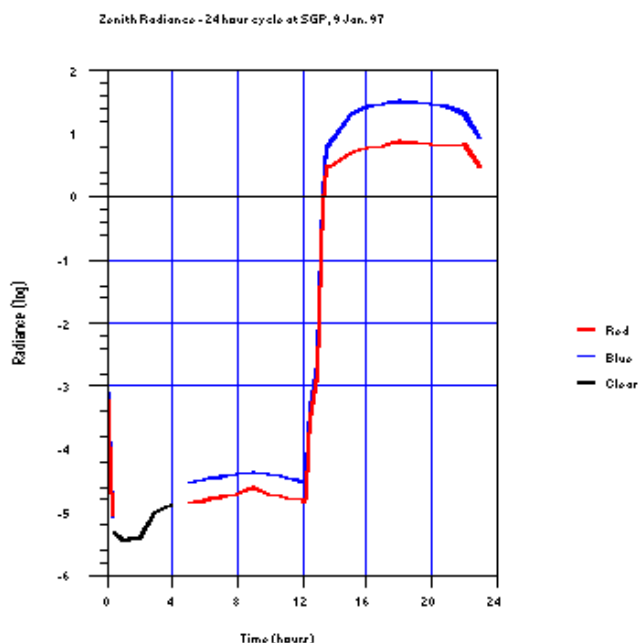
Figure 4. Absolute radiance near the zenith over a 24-hour period. (For a color version of this figure, please see *http://www.arm.gov/docs/documents/ technical/conf_9803/shields-98.pdf.*)

As a first "sanity check," we have compared these radiances with radiances obtained by the MPL using scanning radiometers in the 1960s and 1970s. The starlight radiance of $3.6 \cdot 10^{-6}$ compares well with the night zenith radiances of $2 - 4 \cdot 10^{-6}$ obtained at night at similar wavelengths (Duntley et al. 1970). The daylight radiances of $9.0 \cdot 10^0$ in the red and $3.5 \cdot 10^1$ in the blue compare reasonably with flight data at a similar scattering angle and similar wavelengths for a sample flight (Johnson et al. 1981) that were $7.1 \cdot 10^0$ to $7.5 \cdot 10^0$ in the red and $3.0 \cdot 10^1$ to $3.2 \cdot 10^1$ in the blue. Clearly, it will be important to make more detailed comparisons with measured and model data, particularly taking into account the atmospheric conditions, as radiances can vary significantly as aerosol amount and character changes.

Comparison with Model

Initial comparison with models has been made using the SBDART model (Ricchiazzi et al. 1995), based on LOWTRAN 7 (Kneizys et al. 1983 and Pierluissi et al. 1989), and DISORT (Stamnes et al. 1988). A comparison was made for September 29, 1997, at 1201 local time, a relatively pristine sky with very little cloud or aerosol. A plot of radiance in a line across the center of the image from horizon to horizon, east to west going through zenith, is shown in Figure 5. In this example, the model data have been processed using a mid-latitude summer atmosphere (McClatchey et al. 1972) modified to be consistent with the nearest rawindsonde launch from the SGP CART site. As shown in this example, the model and measured radiances match well at the zenith and show a systematic divergence near the horizons.
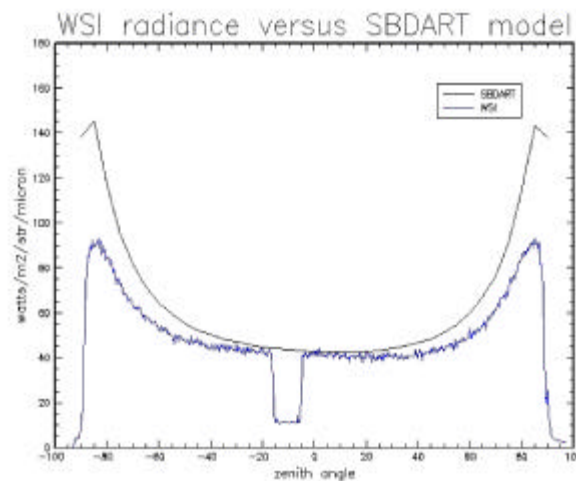

Figure 5. Model radiances and measure radiances for September 29, 1997. (For a color version of this figure, please see *http://www.arm.gov/docs/ documents/technical/conf_9803/shields-98.pdf.*)

In the near future, we will be evaluating the radiances, both against model data and against radiances acquired with a scanning radiometer system in order to evaluate the data. This will be part of the "sanity check" on the calibration procedure and results.

Cloud Decision Algorithms

As noted in the "Recent WSI Upgrades and Progress" section, the current cloud algorithm provides cloud decision images with both opaque and thin cloud determinations, as shown in Figure 2, but the reported cloud fractions only report the opaque cloud determination results. The opaque cloud decision algorithm is based on the red/blue ratios, and

the thin cloud decision algorithm is based on the ratio between the red/blue ratios and clear-day red/blue ratios. An example of a thin cloud determination is shown in Figure 6. This thin cloud determination is not yet included in the cloud fraction reports because it does not yet include a time varying factor to account for variations in haze amount, which are known to impact this algorithm.
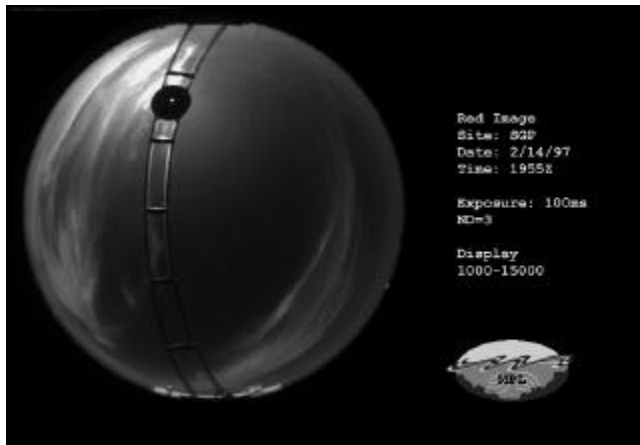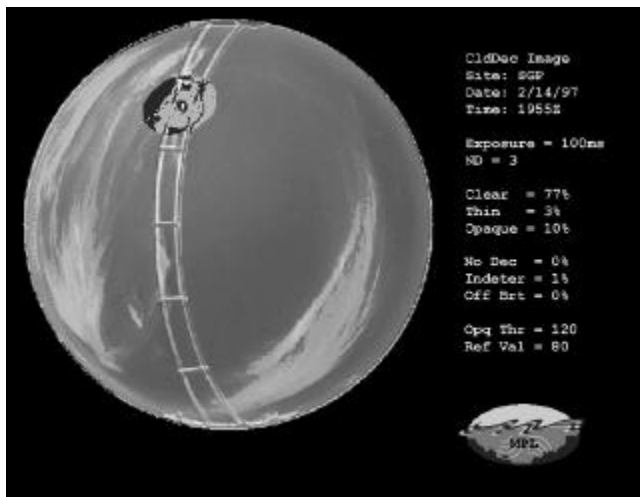

Figure 6a. Raw red image for a sky with thin clouds.

Figure 6b. Grey rendition of cloud decision image for a sky with thin clouds.

In order to address improved cloud algorithms, SNL and Mission Research Corporation (MRC) are evaluating an alternative approach that also makes use of the calibrated radiances. In this approach, the radiances are normalized with respect to the radiances at the same solar zenith angle and look angle on a pristine day. In Figure 7, these normalized radiances are plotted with log red' on the x axis, log blue' on the y axis, and number density indicated by color, where red' and blue' are the normalized red and blue

radiances in a given pixel. Data corresponding to clear sky or haze tend to fall to the right of a line defined by log blue' = .915 log red' + C, and the thin cloud data tend to fall to the left of this line. By comparison, the existing algorithm for thin clouds, which identifies thin clouds by their red/blue ratio and its comparison with the red/blue ratio on a clear day, would correspond to the equation log blue' = log red' + C where C is time varying as a function of haze amount.
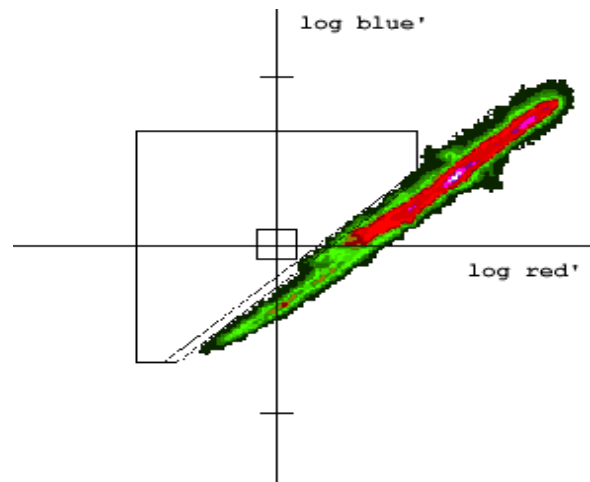

Figure 7a. Normalized radiance distribution on three cloudy days. (For a color version of this figure, please see *http://www.arm.gov/docs/documents/technical/conf_9803/shields-98.pdf*.)
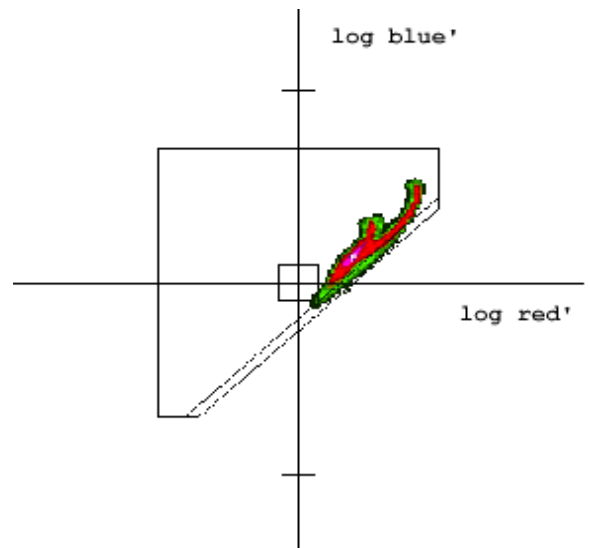

Figure 7b. Normalized radiance distribution on two "aerosol" days. (For a color version of this figure, please see *http://www.arm.gov/docs/documents/technical/conf_9803/shields-98.pdf*.)

For an initial evaluation, thin clouds have been defined as pixels with red' less than .2 or greater than 5, or blue' less than .2 or greater than 5, or log blue' less than .915 log red' -5. Thus, for this test case, we have included pixels with a red or blue radiance significantly different from a pristine day as cloud, in addition to those cases identified as thin cloud by their red/blue ratio. The thin cloud result is shown in Figure 8. Work to evaluate these approaches and yield an improved thin cloud algorithm is currently under way at MRC. In addition, we are planning some changes to constant input to the opaque cloud decision algorithm, as it is not handling the horizon correctly at the present time under overcast conditions.
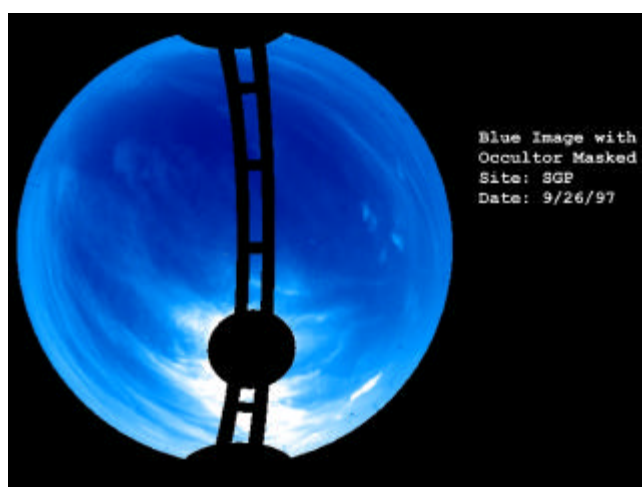

Figure 8a. Blue image with occultor masked out. (For a color version of this figure, please see *http://www.arm.gov/docs/documents/technical/conf_98 03/shields-98.pdf.*)
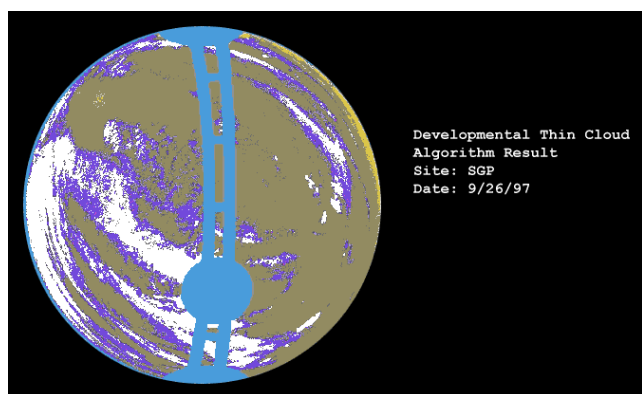

Figure 8b. Sample developmental algorithm result, showing a gray rendition of the colored cloud decision image from September 26, 1997. (For a color version of this figure, please see *http://www.arm.gov/docs/ documents/technical/conf_9803/shields-98.pdf.*)

Work has also begun on a cloud decision algorithm for night skies. Prior to the ARM Program, MPL developed a moonlight algorithm that was quite effective in test cases but has not been evaluated for more extensive cases. The atmospheric radiance is quite different under starlight, and MPL has recommended using another approach such as star counting. MRC, SNL, and MPL are collaborating on a night algorithm based on the detection of stars. Figure 9 shows a plot of a 30 x 30 pixel region around a star field both with and without thin clouds. In the case with clouds,
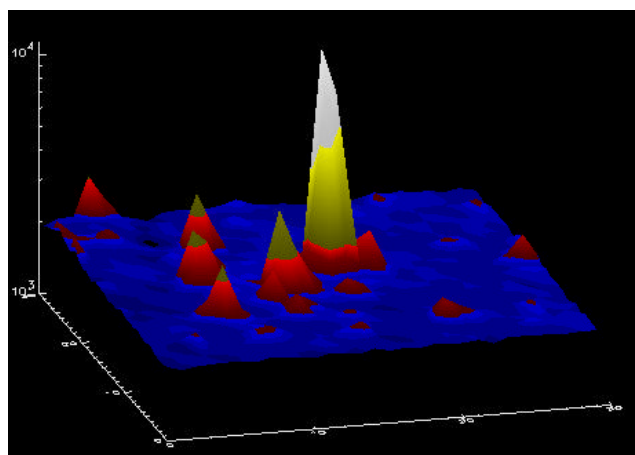

Figure 9a. Radiance field at night on December 18, 1997. This 30 x 30 pixel region near Aldebaran in the Taurus constellation is shown on a relatively clear night. (For a color version of this figure, please see *http://www.arm.gov/docs/documents/technical/conf_98 03/shields-98.pdf.*)
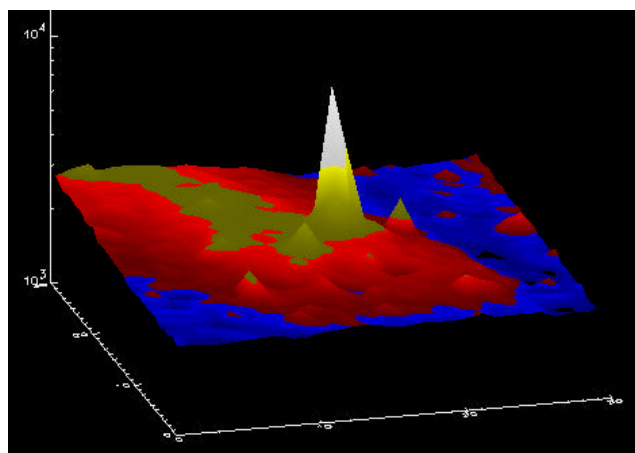

Figure 9b. Radiance Field on December 18, 1997, with semi-transparent clouds. (For a color version of this figure, please see *http://www.arm.gov/docs/ documents/technical/conf_9803/shields-98.pdf.*)

the magnitude of the star signal has decreased, some of the less bright stars have receded into the background, the background radiance has increased, and the spatial texture of the background radiance has changed. We feel that these should provide adequate cues to automated determination of the presence of the stars.

As an initial start on the night algorithm, SNL has devised an improved geometric calibration based on the known position of stars in one image. With the new mapping equations, it is possible to map the star positions onto an image at an arbitrary time with a median accuracy of approximately .1 pixel, with a few outliers of a pixel or two. Figure 10 shows a plot of the star locations generated by this mapping procedure superimposed on the stars in an acquired image. The initial approach to the algorithm will be to map the star position into the image frame, then detect the presence or absence of these stars in the acquired image. If the star or other sky object is not found or the object is dimmer than expected, clouds or aerosols may be present. Repeating the process, looking for fainter objects, may provide information about the optical depth.

Figure 10. Star mapping of Orion constellation onto CCD chip. In this roughly 30 x 30 pixel region, "+" shows the anticipated locations based on lens calibration, and gray boxes show star images.

Summary

As the availability of the WSI data products continues to increase, we feel that the day/night WSI data will have significant potential applications. The instrument yields cloud fraction and the distribution of clouds over the sky dome, as well as the associated distribution of the radiance. Interest areas identified by the Clouds Working Group related to the WSI include several areas: relating cloud fraction and downward direct and diffuse flux, studies of clear sky radiance distribution and its relation to the aerosols, and cloud field geometry in comparison with the cloud field geometry generated by 3D cloud resolving models.

References

Duntley, S. Q., R. W. Johnson, J. I. Gordon, and A. R. Boileau, 1970: Airborne measurements of optical atmospheric properties at night. University of California, San Diego, Scripps Institution of Oceanography, Visibility Laboratory, SIO 70-7. AFCRL-70-0137.

Johnson, R. W., and W. S. Hering, 1981: An analysis of natural variations in European sky and terrain radiance measurements. University of California, San Diego, Scripps Institution of Oceanography, Visibility Laboratory, SIO 82-6. AFGL-TR-81-0317.

Johnson, R. W., W. S. Hering, and J. E. Shields, 1989: Automated visibility and cloud cover measurements with a solid-state imaging system. University of California, San Diego, Scripps Institution of Oceanography, Marine Physical Laboratory.

Johnson, R. W., J. E. Shields, and T. L. Koehler, 1991: Analysis and interpretation of simultaneous multi-station whole sky imagery. University of California, San Diego, Scripps Institution of Oceanography, Marine Physical Laboratory. SIO 91-33. PL-TR-91-2214.

Kneizys, F. X., E. P. Shettle, W. O. Gallery, J. H. Chetwynd, L. W., Abreu, J. E. A. Selby, S. A. Clough, and R. W. Fenn, 1983: Atmospheric transmittance/radiance: computer code LOWTRAN 6. Air Force Geophysics Laboratory, Report AFGL-TR-83-0187, Hansco Air Force Base, Massachusetts.

McClatchey, R. A., R. W. Fenn, J. E. A. Selby, F. E. Volz, and J. S. Garing, 1972: Optical properties of the atmosphere, (third edition). Air Force Cambridge Research Laboratories, Report AFCRL-72-0497.

Pierluissi, J. H., C. E. Maragoudakis, and R. Tehrani-Movahed, 1989: New LOWTRAN band model for water vapor. *Applied Optics*, **28**(18), pp. 3792-3795.

Ricchiazzi P., C. Gautier, and D. Lubin, 1995: Cloud scattering optical depth and local al surface albedo in the Antarctic: Simultaneous retrieval using ground-based radiometry. *JGR*, **100**(D10), 21091-21104.

Shields, J. E., R. W. Johnson, and T. L. Koehler, 1993: Automated whole sky imaging systems for cloud field assessment. Fourth Symposium Of Global Change Studies. January 17-22, 1993. American Meteorological Society, Boston, Massachusetts.

Shields, J. E., R. W. Johnson, M. E. Karr, and J. L. Wertz, 1998: Automated day/night whole sky imagers for field assessment of cloud cover distributions and radiance distributions. Tenth Symposium on Meteorological Observations and Instrumentation. January 11-16, 1998. American Meteorological Society, Phoenix, Arizona.

Stamnes, K., S.-C. Tsay, W. J. Wiscombe and K. Jayaweera, 1988: Numerically stable algorithm for discrete-ordinate-method radiative transfer in multiple scattering and emitting layered media. *Appl. Opt*., **27**, 2502-2509.